The Astrophysical Journal, 893:168 (8pp), 2020 April 20 https://doi.org/10.3847/1538-4357/ab7db4


# $H_2O_2$-induced Greenhouse Warming on Oxidized Early Mars

Yuichi Ito[1,2], George L. Hashimoto[3], Yoshiyuki O. Takahashi[4], Masaki Ishiwatari[2], and Kiyoshi Kuramoto[2]
[1] Department of Physics and Astronomy, University College London, London WC1E 6BT, UK; yuichi.ito.kkyr@gmail.com
[2] Department of Cosmosciences, Hokkaido University, Sapporo 060-0810, Japan
[3] Department of Earth Sciences, Okayama University, Okayama 700-8530, Japan
[4] Department of Planetology, Kobe University, Kobe 657-8501, Japan
*Received 2019 August 1; revised 2020 February 25; accepted 2020 March 5; published 2020 April 28*

## Abstract

The existence of liquid water within an oxidized environment on early Mars has been inferred by the Mn-rich rocks found during recent explorations on Mars. The oxidized atmosphere implied by the Mn-rich rocks would basically be comprised of $CO_2$ and $H_2O$ without any reduced greenhouse gases such as $H_2$ and $CH_4$. So far, however, it has been thought that early Mars could not have been warm enough to sustain water in liquid form without the presence of reduced greenhouse gases. Here, we propose that $H_2O_2$ could have been the gas responsible for warming the surface of the oxidized early Mars. Our one-dimensional atmospheric model shows that only 1 ppm of $H_2O_2$ is enough to warm the planetary surface because of its strong absorption at far-infrared wavelengths, in which the surface temperature could have reached over 273 K for a $CO_2$ atmosphere with a pressure of 3 bar. A wet and oxidized atmosphere is expected to maintain sufficient quantities of $H_2O_2$ gas in its upper atmosphere due to its rapid photochemical production in slow condensation conditions. Our results demonstrate that a warm and wet environment could have been maintained on an oxidized early Mars, thereby suggesting that there may be connections between its ancient atmospheric redox state and possible aqueous environment.

*Unified Astronomy Thesaurus concepts:* Inner planets (797); Mars (1007); Planetary atmospheres (1244)

## 1. Introduction

One of the most intriguing and debatable problems in planetary science is elucidating how an early Martian surface environment could have been warm enough to sustain liquid water (Wordsworth 2016; Ramirez & Craddock 2018). Climate models have shown that a $CO_2$–$H_2O$ atmosphere alone could not have kept early Mars warm enough to sustain liquid water globally even if any amount of atmospheric pressure is assumed (e.g., Kasting 1991). This suggests that the other greenhouse components could have played a key role in the early Martian atmosphere. Current theoretical models suggest that the warming of early Mars was caused by a $CO_2$–$H_2O$ atmosphere combined with additional greenhouse substances: clouds (e.g., Forget & Pierrehumbert 1997; Wordsworth et al. 2013); reducing gases such as $H_2$, $CH_4$, and $NH_3$ (e.g., Sagan & Mullen 1972; Kasting et al. 1992; Ramirez et al. 2014; Ramirez 2017; Wordsworth et al. 2017); and/or volcanic gases such as $H_2S$ and $SO_2$ (e.g., Postawko & Kuhn 1986; Johnson et al. 2008; Tian et al. 2010).

Recently, NASA's Curiosity rover discovered a high abundance of Mn in sedimentary rocks (Lanza et al. 2016). During the era in which the observed Mn-oxide-rich rocks at Gale crater would have precipitated out, Mars may have had both liquid water on its surface and a highly oxidized atmosphere (Lanza et al. 2016; Noda et al. 2019). Furthermore, the existence of rocks with a high concentration of Mn at Endeavour crater (Arvidson et al. 2016) suggests that such an oxidized and wet surface environment was a global phenomenon at that time. These findings suggest that the early Martian surface had once experienced a wet and warm environment, but with the absence of reduced gas species that would have enhanced the greenhouse effect of a $CO_2$–$H_2O$ dominated Martian atmosphere to allow the existence of liquid water. One might consider $SO_2$ as a candidate greenhouse gas in an oxidized atmosphere (e.g., Johnson et al. 2008), but its presence seems unlikely during this era because Mn and S are not correlated in the rocks found at Gale crater (Lanza et al. 2016).

In an attempt to address this uncertainty, in this study we investigate the greenhouse effect due to hydrogen peroxide ($H_2O_2$) gas in the early Martian atmosphere. Previously, it had been proposed that $H_2O_2$ gas was responsible for oxidizing the early Martian surface (e.g., Zahnle et al. 2008). Although the idea that $H_2O_2$ was one of the greenhouse gases responsible for the warming of early Mars has widely been ignored, $H_2O_2$ does absorb radiation at wavenumbers near 500 $cm^{-1}$, where the blackbody radiation at a temperature of 250 K has peak intensity and $CO_2$ has an absorption window, as shown in Figure 1 (see also Figure 4 in Wordsworth 2016). Also, the absorption cross section of $H_2O_2$ is larger than those of known greenhouse gases such as $SO_2$, $NH_3$, $CH_4$, and OCS in a wavenumber range from 250–450 $cm^{-1}$, as shown in Figure 2.

The remainder of this paper is organized as follows. In Section 2, we describe our atmospheric model and numerical setup. In Section 3 we show the surface temperature as a function of $H_2O_2$ abundance under the conditions that may have been present on early Mars. We discuss the photochemical production and condensation of $H_2O_2$ in a warm and wet early Martian atmosphere and the possible warming scenario of $H_2O_2$ in an oxidized early Martian environment in Section 4. Finally we summarize our results in Section 5.

## 2. Atmospheric Model

We set up a vertical, one-dimensional $CO_2$-dominant atmospheric model and determine the surface temperature required to achieve balance between the absorbed solar radiation and the outgoing planetary radiation with approximated radiative–convective equilibrium temperature–pressure profiles and given compositions. The numerical scheme is based on the same line-by-line calculations used in the

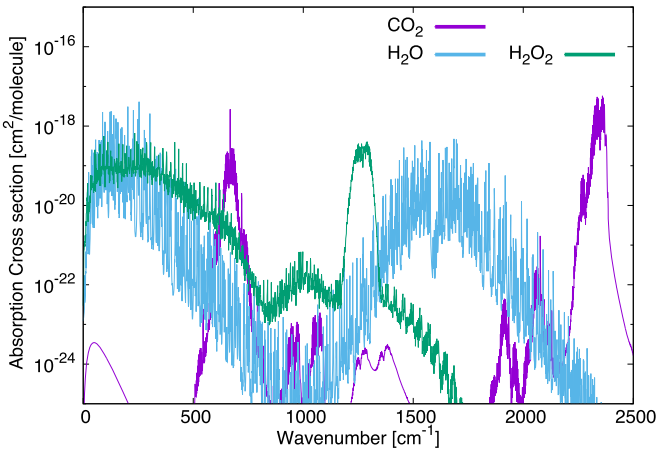


**Figure 1.** Absorption cross sections of three oxidized gases, $CO_2$ (magenta), $H_2O$ (cyan), and $H_2O_2$ (green) at 250 K and 1 bar, as functions of wavenumber. These cross sections are produced using the line profile calculation code EXOCROSS (Yurchenko et al. 2018). The absorption data and the assumed line profiles are described in Section 2.

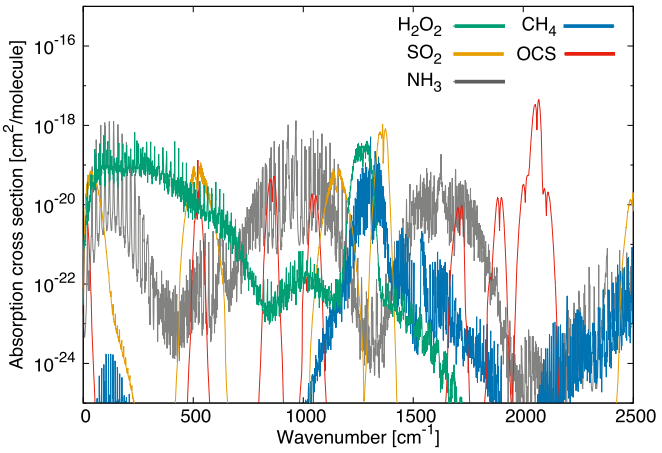


**Figure 2.** Absorption cross sections of $H_2O_2$ (green) and four greenhouse gases, $SO_2$ (orange), $NH_3$ (gray), $CH_4$ (blue), and OCS (red) at 250 K and 1 bar, as functions of wavenumber. These cross sections are calculated using EXOCROSS (Yurchenko et al. 2018) and HITRAN2012 (Rothman et al. 2013), assuming a Voigt profile truncated at 25 $cm^{-1}$ from the line center.

calculations of the surface temperature warmed by $H_2O$ (Schaefer et al. 2016) and $CO_2$–$H_2$–$CH_4$ atmospheres (Wordsworth et al. 2017).

The atmosphere in hydrostatic equilibrium is vertically divided into 100 layers from the ground to the top of the atmosphere ($1 \times 10^{-4}$ bar for the model atmosphere). The surface pressure ranges from 0.01 to 3 bar. The vertical grid of the atmosphere is set so that the logarithms of pressure are evenly spaced. Following previous models (Ramirez et al. 2014; Ramirez 2017), we set the modeled atmosphere to one composed of 95% $CO_2$, fully saturated $H_2O$, fully saturated or different mixing ratios of $H_2O_2$, and $\leqslant$5% $N_2$. For the saturated $H_2O_2$ amount, we calculate the vapor pressure using the Clausius–Clapeyron equation. Then, we use the thermal properties of $H_2O_2$ (Foley & Giguére 1951a) and its saturation vapor pressure of $4.69 \times 10^{-4}$ bar at the melting point (272.69 K) as a reference pressure (Manatt & Manatt 2004). In the other cases, the molar fraction of $H_2O_2$ is assumed to be vertically constant and its value was in the range from 10 ppb to 10 ppm. Additionally, the abundance of $H_2O$ is determined by the saturation vapor pressure of water (Equations (11) and (12) in Kasting et al. 1984).

The atmospheric temperature profile is assumed to be that of a moist adiabat of $H_2O$ and $CO_2$ from the surface to the tropopause and an isothermal stratosphere above the tropopause. Using the heat capacity, $c_p$, given by the Shomate equation,[5] the vapor amount and latent heat of $H_2O$ (Equation (12) in Kasting et al. 1984) and the gravity of Mars, $g$, the moist adiabat of $H_2O$ is given by Equation (2.48) in Andrews (2000). Decreasing gravity with altitude is included in this model. The moist adiabat of $CO_2$ is adopted where the moist adiabat of $H_2O$ is colder than the saturation vapor pressure of $CO_2$ using Equations (A5) and (A6) in Kasting (1991). We assume that the stratospheric temperature is 155 K ($\sim$167 K $\times$ $0.75^{1/4}$), which is based on the results of Kasting (1991), who uses 167 K as the stratospheric temperature for current solar heating and scales it for different solar heating rates by assuming that the stratospheric temperature is proportional to the skin temperature.

Using the atmospheric structure described above, we calculate the outgoing planetary radiation based on a line-by-line radiative transfer calculation. The outgoing planetary radiation is given by

$$F_p = 2\pi \int B_\nu(T_{\rm surf}) \int_0^1 \mu e^{-\tau_{\nu,{\rm surf}}/\mu} d\mu d\nu + 2\pi \int \int_0^{\tau_{\nu,{\rm surf}}} \int_0^1 B_\nu(t_\nu) e^{-\tau_\nu/\mu} d\mu d\tau_\nu d\nu, \quad (1)$$

where $T_{\rm surf}$ is the surface temperature, $\mu$ is the cosine of the zenith angle, $B_\nu$ is the Planck function at wavenumber, $\nu$, and $\tau_\nu$, surf is the total optical depth of the atmosphere. In hydrostatic equilibrium, the optical depth is given by

$$\frac{d\tau_\nu}{dP} = \frac{\sum \chi_A \sigma_{\nu,A}}{\bar{m} g}, \quad (2)$$

where $P$ is atmospheric pressure, $\bar{m}$ is the mean mass of the atmospheric gas particles, and $\chi_A$ and $\sigma_{\nu,A}$ are the molar fraction and absorption cross section of an absorber $A$, respectively. Following Ramirez (2017) and Kopparapu et al. (2013), the line absorption cross section profile of $CO_2$ is assumed to be a sub-Lorentzian (Perrin & Hartmann 1989) truncated at 500 $cm^{-1}$ from the line center, while that of $H_2O$ is assumed to be a Voigt profile truncated at 25 $cm^{-1}$ from the line center. The line profile of $H_2O_2$ is also assumed to be a Voigt profile truncated at 25 $cm^{-1}$ from the line center. For the line absorption of each gas species, the line data given by HITRAN2012 (Rothman et al. 2013) and the line profile calculation code EXOCROSS (Yurchenko et al. 2018) are used in this model. Additionally, the collision-induced absorption of $CO_2$–$CO_2$ (Gruszka & Borysow 1997; Baranov et al. 2004) is considered. In practice, to save memory and CPU time, we have prepared a numerical table in which the absorption cross sections are given as functions of temperature, $T$, and $\log_{10} P$. The table was created using values of $T$ = 150, 200, 250, 300, and 350 K, and $\log_{10}(P/{\rm bar})$= $-4$, $-3$, $-2$, $-1$, 0, and 1. We evaluate the integral shown in Equation (1) over a wavenumber range from 1 to 10,000 $cm^{-1}$ with a resolution of 1 $cm^{-1}$. The numerical integration of Equation (1) with respect to the zenith

[5] http://old.vscht.cz/fch/cz/pomucky/fchab/Shomate.html

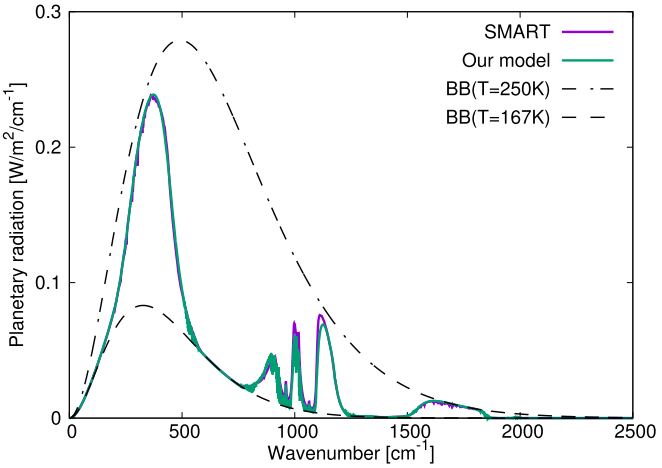


**Figure 3.** Outgoing planetary radiation as a function of wavenumber for a dry, 2 bar $CO_2$ atmosphere, comparing the result calculated by our line-by-line model (green) against the result produced with the SMARTS code (violet). In each model, a dry $CO_2$(95%)–$N_2$(5%) atmosphere with a pressure of 2 bar, a surface temperature of 250 K, and a stratospheric temperature of 167 K is assumed. Also, the assumed temperature profile follows the dry and moist adiabatic lapse rate of $CO_2$. The plotted SMART data are the same with those shown in Figure S2 of Ramirez et al. (2014). The black dashed curves show blackbody radiation, of which the temperatures are indicated by BB($T$).

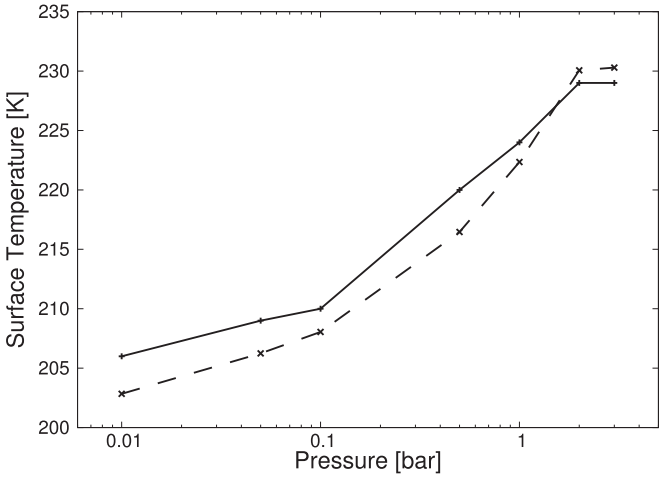


**Figure 4.** Surface temperature as a function of surface pressure for wet $CO_2$(95%)–$N_2$(5%) atmospheres, comparing the result calculated by our model (solid) against the result of Ramirez et al. (2014) (dotted).

angle is performed using the exponential integral calculation code presented by Press et al. (1996), while the other integrals are evaluated using trapezoidal integration.

We iteratively determine the surface temperature at which the outgoing planetary radiation balances the absorbed solar radiation. The absorbed solar radiation is given by $(1-A_p)F_{\rm sol}/4$, where $A_p$ is the planetary albedo and $F_{\rm sol}$ is the solar flux. The solar flux is assumed to be $F_{\rm sol} = 590 \times 0.75$ W m$^{-2}$, and we use the planetary albedo of a wet $CO_2$(95%)–$N_2$(5%) atmosphere not warmed by any additional greenhouse mechanism (Ramirez et al. 2014). Note that our assumed planetary albedo underestimates the surface temperature in a warm atmosphere with enhanced saturated-$H_2O$ content more than the atmosphere not warmed by $H_2O_2$. This is because the absorption of solar radiation by $H_2O$ decreases the planetary albedo (Kasting 1988), and $H_2O_2$ might work in the same way. While the Rayleigh scattering cross section per a $H_2O_2$ molecule is comparable with that of $CO_2$ based on its electric dipole polarizability (Maroulis 1992), the abundance of $H_2O_2$ in our model is too low (up to 10 ppm) to increase the planetary albedo. Also, though there is no public absorption data of $H_2O_2$ in the optical regime (see Al-Refaie et al. 2016; Tennyson & Yurchenko 2018), its absorption in the optical is likely to not be very strong (see also the MPI–Mainz UV/VIS Spectral Atlas[6]; Keller-Rudek et al. 2013).

### 2.1. Model Validation

We have performed two benchmark tests of our simulation code, and we have confirmed that our model reproduce the numerical solutions for the dry and wet $CO_2$-rich atmospheres of early Mars shown in Ramirez et al. (2014).

We first compare our line-by-line model against a well-tested line-by-line model, SMART (Meadows & Crisp 1996), for a dry, 2 bar $CO_2$(95%)–$N_2$(5%) atmosphere. With the same temperature profile shown in Figure S1 of Ramirez et al. (2014), we calculated the outgoing planetary radiation using our model. Figure 3 shows a comparison between the SMART result and that from our model. Our model spectra agree well with the SMART spectra, although there is some difference in the wavenumber region from 800–1200 cm$^{-1}$, which is likely due to the different absorption data used in both studies. The total flux of our model is 87.2 W m$^{-2}$, which agrees well with that found by SMART (88.4 W m$^{-2}$). Note that the calculated fluxes differ by at most 0.05%, even if we double the resolution of the wavenumber or the number of vertical layers.

Next, we compare the surface temperatures of a wet, 2 bar $CO_2$(95%)–$N_2$(5%) atmosphere with that calculated by the one-dimensional radiative–convective model (Ramirez et al. 2014). Our results agree well with those of Ramirez et al. (2014), as shown in Figure 4, where the differences in the calculated surface temperatures are no more than 4 K. Because the results of our models agree to within 2% of the previous studies, we have confirmed that our model is consistent with these models.

## 3. Results

Figure 5(a) shows the outgoing planetary radiation for a fixed surface pressure and temperature of 2 bar and 273 K, respectively. When the atmosphere consists of $H_2O$ and $CO_2$ (cyan), there are atmospheric windows at wavenumbers below 500 cm$^{-1}$ and around 1000 cm$^{-1}$, which are consistent with the results of previous climate models (e.g., Wordsworth 2016; Ramirez 2017). The addition of $H_2O_2$ reduces the planetary radiation at wavenumbers below 500 cm$^{-1}$ due to its strong far-infrared absorption (blue, olive, green). Although $H_2O_2$ effectively absorbs photons with wavenumbers around 1200 cm$^{-1}$ (Figure 1), this only slightly affects the outgoing planetary radiation because $CO_2$ also absorbs photons at the same wavenumbers.

The outgoing planetary radiation is 87.6 W m$^{-2}$ for an $H_2O_2$-free atmosphere (cyan), which decreases drastically when $H_2O_2$ is added. For vertically constant molar fractions of 1 ppm (olive) and 10 ppm (green) of $H_2O_2$, the outgoing planetary radiation is 68.8 W m$^{-2}$ and 56.5 W m$^{-2}$, respectively. If the abundance of $H_2O_2$ can be constrained by the saturation vapor pressure, the planetary radiation is 84.2 W m$^{-2}$ (blue), and the greenhouse effect of $H_2O_2$ is unremarkable. This is because the abundance of saturated $H_2O_2$

[6] http://satellite.mpic.de/spectral_atlas/index.html

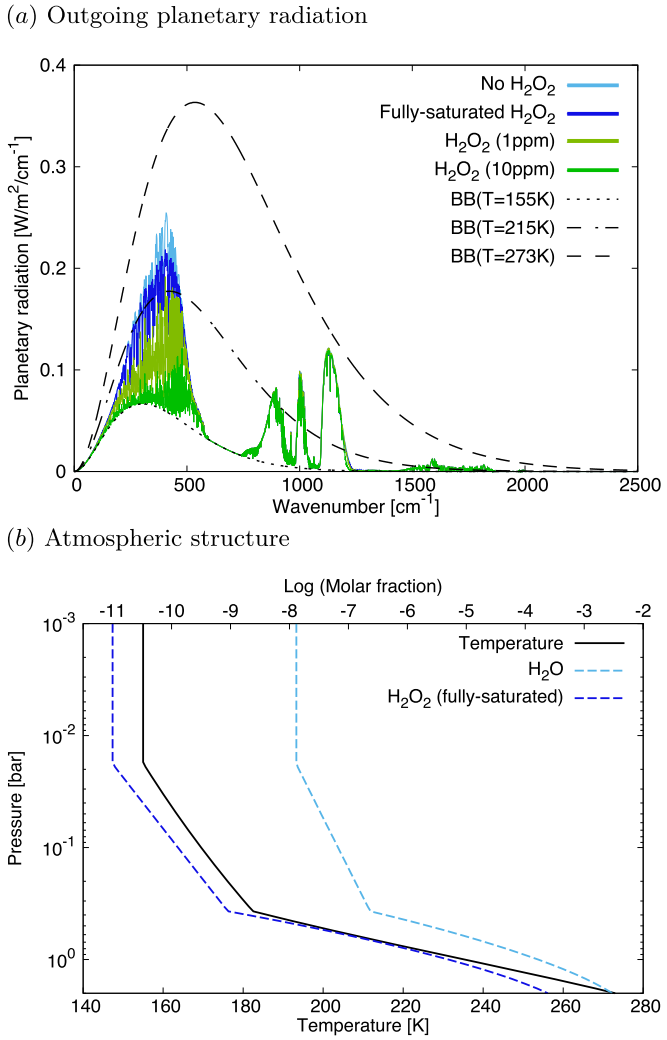


**Figure 5.** Impact of $H_2O_2$ on the outgoing planetary radiation for a surface pressure of 2 bar and a surface temperature of 273 K. (a) The outgoing planetary radiation as a function of wavenumber for the atmospheres without $H_2O_2$ and with different amounts of $H_2O_2$. The black dashed curves show the blackbody radiation, the temperatures of which are indicated, BB($T$). (b) The temperature–pressure profile and the vertical distributions of $H_2O$ and saturated $H_2O_2$ in the atmosphere.

is too low in the low-pressure region to absorb photons effectively (Figure 5(b)).

Next, Figure 6 shows the surface temperature as a function of surface pressure. The differences in surface temperatures between the atmospheres without $H_2O_2$ (black) and with saturated $H_2O_2$ (blue) are at most 4 K. However, in the case of abundant $H_2O_2$, the planetary surface is warm enough to sustain liquid water (Figure 6). In particular, for the 2 bar atmosphere with added 1 ppm (olive) or 10 ppm (green) of $H_2O_2$, the surface temperature increases by about 40 or 65 K from that of the $H_2O_2$-free case (∼230 K), respectively. Our results show that a concentration of only 1 ppm level of $H_2O_2$ is sufficient to effectively cut off the outgoing planetary radiation and warm the planetary surface to temperatures above 273 K. Note that this $H_2O_2$ is supersaturated at high altitudes. For example, in the 2 bar atmosphere, 1 ppm of $H_2O_2$ is supersaturated below the pressure level of ∼0.8 bar, and its supersaturation ratio is as high as $10^5$ at high altitudes where the pressure is ∼0.02 bar or less (see the fully saturated $H_2O_2$ concentration shown in Figure 5(b)). Condensation of $H_2O_2$ in the high-altitude atmosphere is discussed in Section 4.2.

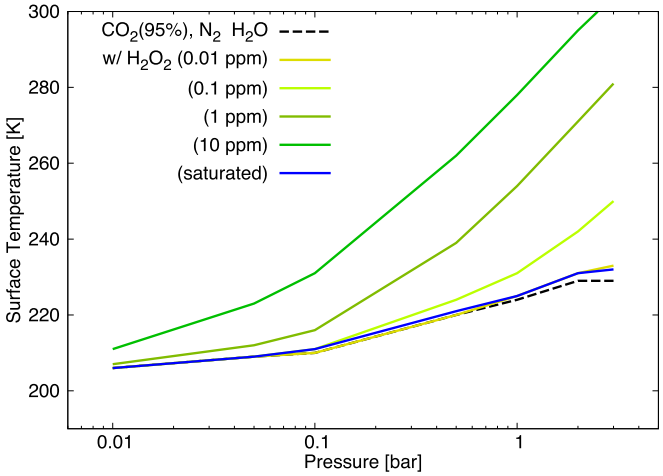


**Figure 6.** Surface temperature as a function of surface pressure. The dashed curve represents the atmosphere without $H_2O_2$ while the solid curves show the atmospheres containing a saturated amount and vertically constant molar fractions of $H_2O_2$. Note that the case of 0.01 ppm of $H_2O_2$ (yellow) is almost identical to those of saturated (blue) and free $H_2O_2$ (black).

## 4. Discussion

### 4.1. $H_2O_2$ in a Wet and Oxidized Atmosphere

$H_2O_2$ is much more abundant in a wet and oxidized atmosphere, though the concentration of $H_2O_2$ in the current dry Martian atmosphere is about 10 ppb (Encrenaz et al. 2004). Although chemical models suggest that the concentration of $H_2O_2$ reaches at most 0.1 ppm in dry atmospheres (Parkinson & Hunten 1972; Gao et al. 2015), a wet and oxidized atmosphere which is suitable for the formation of $H_2O_2$ would contain it in a concentration higher than 0.1 ppm. This is because $H_2O_2$ is produced through the chemical reactions of $HO_x$ gas species such as H, OH, and $HO_2$ which originate from $H_2O$. Also, the abundance of $H_2O_2$ would be higher in an oxidized atmosphere because such an atmosphere inhibits the regeneration of $H_2O$ from $HO_x$ and enhances the production of $H_2O_2$.

In a wet and oxidized Martian atmosphere, the photolysis of $H_2O_2$ is considered to be an effective pathway to regenerate $CO_2$ (Yung & Demore 1999). This regeneration is necessary because $CO_2$ is destroyed by far-UV irradiation ($\lambda \leqslant 227.5$ nm) from the Sun via

$$CO_2 + h\nu \rightarrow CO + O. \quad \text{(R1)}$$

Indeed $CO_2$ regeneration is required to maintain the $CO_2$ atmosphere over geological timescales. In a wet atmosphere, $H_2O_2$ can be sufficiently produced as an intermediate product through the following catalytic cycle:

$$2(H + O_2 + M \rightarrow HO_2 + M), \quad \text{(R2)}$$

$$2HO_2 \rightarrow H_2O_2 + O_2, \quad \text{(R3)}$$

$$H_2O_2 + h\nu \rightarrow 2OH, \quad \text{(R4)}$$

$$2(OH + CO \rightarrow CO_2 + H), \quad \text{(R5)}$$

$$2CO + O_2 \rightarrow 2CO_2. \quad \text{(S1)}$$

Meanwhile, although a thick and dry $CO_2$-rich atmosphere is unstable (Zahnle et al. 2008), in a wet and oxidized atmosphere

of early Mars, $CO_2$ could have been stabilized by S1 (= R2 + R3 + R4 + R5) even if the atmosphere was thick.

We estimate the $H_2O_2$ abundance in a warm/wet and oxidized $CO_2$ atmosphere by assuming that S1 is the cycle most responsible for the regeneration of $CO_2$ against losses due to R1. We assume that the bulk $CO_2$ abundance in the atmosphere is in balance between its photodissociation flux (R1), and twice the $H_2O_2$ photodissociation flux (R4) that produces OH for oxidizing CO. Also, it is assumed that there is no optical shielding effect for photons with wavelengths longer than the shielded wavelength, $\lambda_{sh}$, but there is complete shielding for all other UV photons to $H_2O_2$, for simplicity. Then, the vertical column density of $H_2O_2$, $\Sigma_{H_2O_2}$, can be written as

$$\Sigma_{H_2O_2} = \frac{\int_{\lambda \leqslant 227.5\,\mathrm{nm}} \hat{F}_\lambda d\lambda}{2\int_{\lambda_{sh}}^{\lambda_{th}} \hat{F}_\lambda \sigma_{diss,\lambda} d\lambda}, \quad (3)$$

where $\hat{F}_\lambda$ is the solar photon flux, and $\sigma_{diss,\lambda}$ and $\lambda_{th}$ are the photodissociation cross section and the threshold wavelength for a photon to effectively dissociate $H_2O_2$, respectively. Owing to the low bonding energy of $H_2O_2$ ($\sim$50 kcal mol$^{-1}$ $\sim$570 nm; Bach et al. 1996), the photodissociation is caused not only by UV but also by visible light photons. Therefore, $H_2O_2$ is not completely shielded from stellar irradiation by $H_2O$, $O_2$, and $CO_2$ (Yung & Demore 1999). On the other hand, a developed $O_3$ layer may shield solar photons with wavelengths $\lesssim$300 nm, as displayed on Earth today. Here we use $\lambda_{sh}$ = 227.5 and 300 nm as fiducial values of a shielded wavelength.

The dissociation cross section of $H_2O_2$ has been measured only for photon wavelengths in the range $\leqslant$410 nm (Kahan et al. 2012) because of the technical problem of measuring small absorption cross sections. Hence, we use $\lambda_{th}$ = 410 nm as a fiducial value of the threshold wavelength. Note that according to Kahan et al. (2012), the photolysis of $H_2O_2$ mainly occurs at photon wavelengths shorter than 350 nm. Therefore, inputting $\lambda_{sh}$ = 227.5 nm, the measured cross section with $\lambda_{th}$ = 410 nm (Lin et al. 1978; Kahan et al. 2012) and the solar spectral irradiance at 4 Ga developed by combining the observed spectrum from the Sun with those of solar-type stars at different ages (Claire et al. 2012) in Equation (3), we find $\Sigma_{H_2O_2} \sim 8 \times 10^{17}$ cm$^{-2}$. When we substitute $\lambda_{sh}$ = 300 nm into Equation (3), we find $\Sigma_{H_2O_2} \sim 5 \times 10^{18}$ cm$^{-2}$. These values change only 10% if the solar spectral irradiance at 3.5 Ga is used instead.

The column densities estimated here are significantly larger than the current typical value of $\sim 2 \times 10^{15}$ cm$^{-2}$, which corresponds to 10 ppb at 6 mbar, in the present-day Martian atmosphere. These large column densities produce optical depths over wavenumbers $\nu$ = 100–500 cm$^{-1}$ of $\tau_\nu$ = 0.003–0.6 for $\lambda_{sh}$ = 227.5 nm and $\tau_\nu$ = 0.02–4 for $\lambda_{sh}$ = 300 nm, assuming a far-infrared absorption cross section of $H_2O_2$, $\sigma_{\nu,H_2O_2} = (0.04\text{–}8) \times 10^{-19}$ cm$^2$, which is shown in Figure 1. Thus, if the other gases such as $O_3$ sufficiently can reduce the photolysis of $H_2O_2$, then the amount of $H_2O_2$ in the atmosphere would be large enough to warm the planetary surface. Note that the column density of $H_2O_2$ estimated by Equation (3) is just a typical value when S1 is the cycle most responsible for the stabilization of $CO_2$, while this value could be increased if the self-shielding effect was taken into account in Equation (3). This is because we impose the restriction that only the OH produced by the photolysis of $H_2O_2$ is used to oxidize CO via R5, but all other reactions which produce and remove OH are ignored. Also, the other process potentially affecting the concentration of $H_2O_2$ is discussed in Section 4.3.

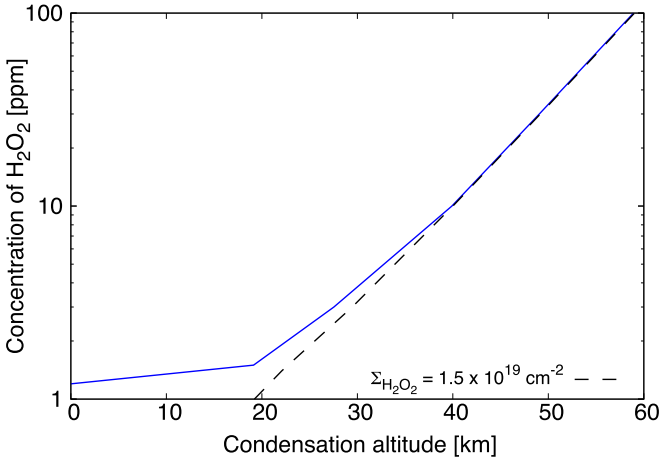


**Figure 7.** The concentration of $H_2O_2$ necessary to warm the planetary surface to 273 K in the 2 bar atmosphere as a function of the condensation altitude (see the text for the definitions of each term). The dashed line represents the column density of $H_2O_2$ with a constant concentration to reach $\Sigma_{H_2O_2}$= $1.5 \times 10^{19}$ cm$^{-2}$.

### 4.2. Condensation of $H_2O_2$

It is likely that $H_2O_2$ in the warm and wet atmosphere of early Mars was supersaturated at high altitudes because the timescale for condensation is likely longer than that for photochemical production. As described later, a timescale for condensation would be much longer than that that governing the production and photodissociation of $H_2O_2$, which was shown by Nair et al. (1994), who used a photochemical model, to be on the order of several hours.

The condensation time can be estimated by assuming that $H_2O_2$ condenses as soon as it collides with condensation nuclei, namely:

$$\tau_{cond} = (4\pi r^2 N_{ccn} \rho v_T)^{-1}, \quad (4)$$

$$\sim 50\ \mathrm{hr} \times \left(\frac{N_{ccn}}{10^5\ \mathrm{kg^{-1}}}\right)^{-1} \left(\frac{P}{0.01\mathrm{bar}}\right)^{-1} \left(\frac{T}{200\ \mathrm{K}}\right)^{\frac{1}{2}} \left(\frac{r}{1\mu\mathrm{m}}\right)^{-2}, \quad (5)$$

where $r$ and $N_{ccn}$ are the size and concentration of the condensation nuclei, respectively, $\rho$ is the atmospheric mass density, and $v_T$ is the thermal velocity of the gas. The timescale for condensation is longer at higher altitudes because the nuclei concentration decreases with increasing altitude. Note that the condensation timescale is underestimated in an atmospheric region with a mean free path smaller than the size of the nuclei (i.e., a dense region) because the diffusive motion of the gas around the nuclei delays the timescale (see Lohmann et al. 2016 for the diffusive case).

Achieving sufficient warming is possible even if $H_2O_2$ condenses at lower altitudes due to the subsequent shorter condensation times. Figure 7 shows the minimum $H_2O_2$ concentration necessary for maintaining a surface temperature of at least 273 K in a 2 bar atmosphere as a function of a

condensation altitude. The condensation altitude stands for an altitude above which the $H_2O_2$ concentration is constant and below which all the $H_2O_2$ gas is virtually removed by rainout through condensation. To warm the surface environment, the required concentration of $H_2O_2$ needs to be about 2 ppm when the condensation altitude is no higher than about 20 km. The 2 ppm of $H_2O_2$ in the upper atmosphere is comparable to $1.5 \times 10^{19}$ cm$^{-2}$, which is also comparable to the $H_2O_2$ column density necessary to stabilize the $CO_2$ atmosphere (Section 4.1). Recent measurements of water vapor in the current Martian upper atmosphere indicate that the supersaturation of water vapor ranges from 1–$10^2$ (Maltagliati et al. 2011; Fedorova et al. 2020), much smaller than $10^5$ that is the supersaturation of 1 ppm $H_2O_2$. However, it should be noted that the mechanism of supersaturation is completely different. On Mars today, the supersaturation of water vapor is generated by the transport of water vapor from the higher temperature region to the lower temperature region. On the other hand, the supersaturation of $H_2O_2$ would be generated by in situ photochemical production with a timescale of several hours. It is likely that the $H_2O_2$ production generates higher supersaturation than that generated by transport, though further studies are needed to quantitatively evaluate the degree of supersaturation.

Warming the planetary surface is still possible if the supersaturation is suppressed to a level of $10^3$. In the 2 bar atmosphere with a surface temperature of 273 K, 1 ppm of $H_2O_2$ makes the outgoing radiation be 68.8 W m$^{-2}$, though the supersaturation is as high as $10^5$ at a higher altitude (see Section 3). When the supersaturation has an upper limit of $S_c = 10^4$, $10^3$, or $10^2$, the outgoing radiation values in our model are 70.5 W m$^{-2}$, 74.5 W m$^{-2}$, or 79.5 W m$^{-2}$, respectively. The upper limit of supersaturation has rather little influence on the outgoing radiation since the photosphere for the wavenumbers of $<500$ cm$^{-1}$ is around a level of 0.3 bar where the supersaturation is $\sim 10^3$. Also, in the case of the 3 bar atmosphere with 1 ppm of $H_2O_2$, $S_c > 2 \times 10^3$ is required to warm the surface temperature above 273 K.

The condensation timescale will not be significantly changed if the dilution effect of $H_2O_2$ in an $H_2O$ solution is taken into account. When the temperature is above $\sim$220 K, an $H_2O$–$H_2O_2$ solution can exist, and then the saturation vapor pressure of $H_2O_2$ will be lowered relative to that of pure $H_2O_2$ (Foley & Giguére 1951b; Manatt & Manatt 2004). However, the temperatures in the photosphere for photons with wavenumbers in the range $\geqslant$500 cm$^{-1}$ are lower than 220 K in thick and warm atmospheres (Figure 5). So it is likely that aqueous solutions would be frozen in the upper atmosphere where the concentration of $H_2O_2$ has the greatest influence on the surface temperature. Therefore, the dilution effect of $H_2O_2$ in an $H_2O$ solution would barely affect the surface temperature. $H_2O_2$ clouds would affect the surface temperature if they are formed. In general, low-altitude clouds can cool the planetary surface and high-altitude clouds can warm the surface (Ramirez & Kasting 2017). It is important to discuss the detail of the $H_2O_2$ cloud radiative forcing but we have left it to the future studies since there is no public refractive index data of $H_2O_2$ particles (see the Refractive Index Database[7]).

[7] https://refractiveindex.info

### 4.3. Other Processes Possibly Affecting $H_2O_2$ Concentration

The atmospheric concentration of $H_2O_2$ can also be affected by several processes such as dissolution into water droplets, dry deposition, and photochemical reactions with volcanic and reactive species (e.g., $SO_2$ and $NO_x$) (Vione et al. 2003).

Although $H_2O_2$ is a minor species, at a level of at most 3.5 ppb in the Earth's atmosphere, which is mainly due to the dissolution of gaseous $H_2O_2$ into water droplets, where $SO_2$ enhances the dissolution rate (Vione et al. 2003), it might not have been a minor species on early Mars during the era in which the observed Mn-oxide-rich rocks at Gale crater would have precipitated out. Since the temperatures at high altitudes in the early Martian atmosphere would be so low that $H_2O$ would freeze, its nondissolution into water droplets would not deplete $H_2O_2$. Meanwhile, at lower altitude regions, $H_2O_2$ would dissolve into water droplets, and precipitation would remove it. If the abundant sulfur-bearing gases were supplied to the early Martian atmosphere, $SO_2$ might have destroyed $H_2O_2$ (e.g., Spracklen et al. 2005; Galeazzo et al. 2018). Although Mn and S are not correlated in the rocks found at Gale crater (Lanza et al. 2016), sulfur deposits are present in large amounts all across the planet and they date to about the same period as Gale crater (e.g., Bibring et al. 2005; Gendrin et al. 2005).

In Earth's atmosphere, dry deposition is another removal process of atmospheric $H_2O_2$ at lower altitudes. The atmospheric $H_2O_2$ of early Mars would be vertically transported by eddy diffusion to the surface, whereby dry deposition and precipitation removed it. For the current Martian atmosphere at altitudes lower than 40 km, the scale height is $H \sim 10$ km and the vertical eddy diffusion coefficient is $K_{ed} \leqslant 10^7$ cm$^2$ s$^{-1}$ (Nair et al. 1994); hence the diffusion timescale is $H^2/K_{ed} \geqslant 1$ day. Since the timescale of $H_2O_2$ photochemical reactions is less than a day (Nair et al. 1994; Zahnle et al. 2008), the atmospheric concentration of $H_2O_2$ at high altitudes is likely to be controlled by photochemical reactions.

The actual eddy diffusion coefficient and dry deposition timescale on early Mars would depend on turbulence/large-scale winds and the compositions/oxidation states of the surface rocks, respectively. As such, a more detailed examination requires that photochemical calculations be done alongside those of the atmospheric thermal structure, which will be the focus of a future study.

### 4.4. Oxidized Early Martian Environment

An early surface environment warmed by the greenhouse effect of $H_2O_2$ (Section 4.1) is consistent with the global, highly oxidized, conditions implied by the high Mn materials found on the Martian surface by the Curiosity rover in Gale crater and by the Opportunity rover in Endeavour crater (Arvidson et al. 2016; Lanza et al. 2016).

The redox state of the early Martian atmosphere was likely controlled by the escape of atmospheric components into space. In the early Martian atmosphere, UV radiation from the young Sun would have enhanced hydrogen escape and effectively oxidized the atmosphere and the surface environment. In addition to hydrogen escape, the escape of atomic carbon might also have contributed to the oxidation of the early Martian atmosphere because its escape flux would not be limited by diffusion in a $CO_2$-rich atmosphere (N. Terada 2020, private communication). Further studies are required to determine the redox state of the early Martian atmosphere, which could also

be affected by the supply of reduced gases (e.g., CO and $H_2$) through volcanic degassing, oxygen escape, and oxygen uptake through weathering of the planetary surface (Zahnle et al. 2008; Wetzel et al. 2013; Batalha et al. 2015).

It is interesting to note that $H_2O_2$ might be able to warm a frozen planet and melt water ice. Liang et al. (2006) demonstrated that a weak hydrological cycle coupled with photochemical reactions could give rise to sustained production of $H_2O_2$ during long and severe glacial intervals. Although an icy surface has a high albedo, the surface temperature can be warmed to temperatures above 273 K by 4 and 15 ppm levels of $H_2O_2$ in a 2 bar atmosphere when the planetary albedo is assumed to be $\leqslant$0.45 and $\leqslant$0.5, respectively, as demonstrated by our model.

It has also been suggested that $H_2O_2$ deposited on the planetary surface could be stored in the ice during the time of a global snowball episode (Liang et al. 2006). If early Mars was once a snowball, and a large amount of $H_2O_2$ was stored in the ice, it would be released into the atmosphere upon melting caused by any mechanism, such as meteor impacts, volcanic emissions, or obliquity changes (e.g., Wordsworth 2016 and references therein). The release of abundant $H_2O_2$ would cause not only a global oxidation event but also enhance greenhouse warming. If so, there might be geological evidence that oxidation and warming occurred simultaneously in the aftermath of a snowball Mars.

## 5. Summary and Conclusion

We investigated the possible impact of $H_2O_2$ as an additional greenhouse gas in a $CO_2$-dominant atmosphere using a one-dimensional atmospheric model. Because the timescale for condensation is longer at higher altitudes (Section 4.2), photochemically-produced $H_2O_2$ would likely be supersaturated in the upper atmosphere. We found that a reasonable amount of $H_2O_2$ in the upper atmosphere effectively cuts off the outgoing planetary radiation in the far-infrared and warms the planetary surface to a temperature hot enough to retain liquid water (Section 3).

Our results demonstrated that a warm and wet surface environment is compatible with an oxidized atmosphere on early Mars. The coexistence of liquid water and an oxidized atmosphere on early Mars has been suggested by the recent discovery of a high level of Mn in some Martian rocks (Arvidson et al. 2016; Lanza et al. 2016). Our results also indicated a key relationship between the redox state of the atmosphere and the surface temperature on early Mars, where the coevolution of these factors may govern the surface environment over geological timescales. This important phenomenon will be the subject of future work, which will aim to understand the surface environment under an oxidized atmosphere on early Mars.

We thank Ramses Ramirez for sharing their albedo spectra and surface temperature data of $CO_2$ atmospheres with us. This work was supported by MEXT/JSPS KAKENHI grant Nos. 17H06457, 18K03719, and 19H01947 and by the NINS Astrobiology Center Project grant No. AB311025.

## ORCID iDs

Yuichi Ito https://orcid.org/0000-0002-0598-3021
George L. Hashimoto https://orcid.org/0000-0002-3821-6881
Yoshiyuki O. Takahashi https://orcid.org/0000-0003-4060-7379
Masaki Ishiwatari https://orcid.org/0000-0001-7490-4676
Kiyoshi Kuramoto https://orcid.org/0000-0002-6757-8064

## References

Al-Refaie, A. F., Polyansky, O. L., Ovsyannikov, R. I., Tennyson, J., & Yurchenko, S. N. 2016, MNRAS, 461, 1012
Andrews, D. G. 2000, An Introduction to Atmospheric Physics (Cambridge: Cambridge Univ. Press)
Arvidson, R. E., Squyres, S. W., Morris, R. V., et al. 2016, AmMin, 101, 1389
Bach, R. D., Ayala, P. Y., & Schlegel, H. B. 1996, JAChS, 118, 12758
Baranov, Y. I., Lafferty, W. J., & Fraser, G. T. 2004, JMoSp, 228, 432
Batalha, N., Domagal-Goldman, S. D., Ramirez, R., & Kasting, J. F. 2015, Icar, 258, 337
Bibring, J.-P., Langevin, Y., Gendrin, A., et al. 2005, Sci, 307, 1576
Claire, M. W., Sheets, J., Cohen, M., et al. 2012, ApJ, 757, 95
Encrenaz, T., Bézard, B., Greathouse, T. K., et al. 2004, Icar, 170, 424
Fedorova, A. A., Montmessin, F., Korablev, O., et al. 2020, Sci, 367, 297
Foley, W. T., & Giguére, P. A. 1951a, CaJCh, 29, 895
Foley, W. T., & Giguére, P. A. 1951b, CaJCh, 29, 123
Forget, F., & Pierrehumbert, R. T. 1997, Sci, 278, 1273
Galeazzo, T., Bekki, S., Martin, E., Savarino, J., & Arnold, S. R. 2018, ACP, 18, 17909
Gao, P., Hu, R., Robinson, T. D., Li, C., & Yung, Y. L. 2015, ApJ, 806, 249
Gendrin, A., Mangold, N., Bibring, J.-P., et al. 2005, Sci, 307, 1587
Gruszka, M., & Borysow, A. 1997, Icar, 129, 172
Johnson, S. S., Mischna, M. A., Grove, T. L., & Zuber, M. T. 2008, JGRE, 113, E08005
Kahan, T. F., Washenfelder, R. A., Vaida, V., & Brown, S. S. 2012, JPCA, 116, 5941
Kasting, J. F. 1988, Icar, 74, 472
Kasting, J. F. 1991, Icar, 94, 1
Kasting, J. F., Brown, L. L., Acord, J. M., & Pollack, J. B. 1992, in Lunar and Planetary Institute Workshop, ed. R. M. Haberle & B. M. Jakosky (Houston, TX: Lunar and Planetary Institute), 84
Kasting, J. F., Pollack, J. B., & Ackerman, T. P. 1984, Icar, 57, 335
Keller-Rudek, H., Moortgat, G. K., Sander, R., & Sörensen, R. 2013, ESSD, 5, 365
Kopparapu, R. K., Ramirez, R., Kasting, J. F., et al. 2013, ApJ, 765, 131
Lanza, N. L., Wiens, R. C., Arvidson, R. E., et al. 2016, GeoRL, 43, 7398
Liang, M.-C., Hartman, H., Kopp, R. E., Kirschvink, J. L., & Yung, Y. L. 2006, PNAS, 103, 18896
Lin, C. L., Rohatgi, N. K., & Demore, W. B. 1978, GeoRL, 5, 113
Lohmann, U., Lüönd, F., & Mahrt, F. 2016, An Introduction to Clouds: From the Microscale to Climate (Cambridge: Cambridge Univ. Press),
Maltagliati, L., Montmessin, F., Fedorova, A., et al. 2011, Sci, 333, 1868
Manatt, S. L., & Manatt, M. R. R. 2004, CEJ, 10, 6540
Maroulis, G. 1992, JChPh, 96, 6048
Meadows, V. S., & Crisp, D. 1996, JGR, 101, 4595
Nair, H., Allen, M., Anbar, A. D., Yung, Y. L., & Clancy, R. T. 1994, Icar, 111, 124
Noda, N., Imamura, S., Sekine, Y., et al. 2019, JGRE, 124, 1282
Parkinson, T. D., & Hunten, D. M. 1972, JAtS, 29, 1380
Perrin, M. Y., & Hartmann, J. M. 1989, JQSRT, 42, 311
Postawko, S. E., & Kuhn, W. R. 1986, JGR, 91, D431
Press, W. H., Teukolsky, S. A., Vetterling, W. T., & Flannery, B. P. 1996, Numerical Recipes in Fortran 77: the Art of Scientific Computing, Vol. 1 (2nd ed.; Cambridge: Cambridge Univ. Press)
Ramirez, R. M. 2017, Icar, 297, 71
Ramirez, R. M., & Craddock, R. A. 2018, NatGe, 11, 230
Ramirez, R. M., & Kasting, J. F. 2017, Icar, 281, 248
Ramirez, R. M., Kopparapu, R., Zugger, M. E., et al. 2014, NatGe, 7, 59
Rothman, L. S., Gordon, I. E., Babikov, Y., et al. 2013, JQSRT, 130, 4
Sagan, C., & Mullen, G. 1972, Sci, 177, 52
Schaefer, L., Wordsworth, R. D., Berta-Thompson, Z., & Sasselov, D. 2016, ApJ, 829, 63
Spracklen, D. V., Pringle, K. J., Carslaw, K. S., Chipperfield, M. P., & Mann, G. W. 2005, ACP, 5, 2227
Tennyson, J., & Yurchenko, S. N. 2018, Atoms, 6, 26
Tian, F., Claire, M. W., Haqq-Misra, J. D., et al. 2010, E&PSL, 295, 412

Vione, D., Maurino, V., Minero, C., & Pelizzetti, E. 2003, Annali di Chimica, 93, 477
Wetzel, D. T., Rutherford, M. J., Jacobsen, S. D., Hauri, E. H., & Saal, A. E. 2013, PNAS, 110, 8010
Wordsworth, R., Forget, F., Millour, E., et al. 2013, Icar, 222, 1
Wordsworth, R., Kalugina, Y., Lokshtanov, S., et al. 2017, GeoRL, 44, 665
Wordsworth, R. D. 2016, AREPS, 44, 381
Yung, Y. L., & Demore, W. B. (ed.) 1999, Photochemistry of Planetary Atmospheres (Oxford: Oxford Univ. Press)
Yurchenko, S. N., Al-Refaie, A. F., & Tennyson, J. 2018, A&A, 614, A131
Zahnle, K., Haberle, R. M., Catling, D. C., & Kasting, J. F. 2008, JGRE, 113, E11004